


Understanding gray track formation in KTP: Ti^{3+} centers studied from first principles

A. Bocchini ^{*}, C. Eigner , C. Silberhorn , W. G. Schmidt , and U. Gerstmann 

Department Physik, Universität Paderborn, Paderborn 33098, Germany

 (Received 2 October 2020; revised 13 November 2020; accepted 17 November 2020; published 4 December 2020)

The magnetic signatures of Ti^{3+} centers in potassium titanyl phosphate (KTP) are studied within density-functional theory (DFT). The hyperfine tensor elements are very sensitive to the structural surrounding; the paramagnetic hyperfine splittings are used to evaluate the defect models. For each of the four experimentally observed electron paramagnetic resonance (EPR) spectra, we identify a defect model that reproduces the paramagnetic signature. All of them are electron donors, whereby one specific Ti atom can be identified, whose formal oxidation number is lowered from 4+ in the ideal crystal to 3+. The related charge redistribution leads to a strong polarization of the corresponding Ti^{3+} center. However, in three cases a second Ti atom, connected to the first by a mutual polarized O atom, is polarized too. Positively charged O vacancies at the lattice site O(10) are unique in leading to the formation of the only Ti^{3+} center that is stable at room temperature. This defect induces a defect state within the band gap, which may be excited during second harmonic generation (SHG) applications and thus is a plausible candidate to explain the so-called gray tracking, i.e., photochromic damage.

DOI: [10.1103/PhysRevMaterials.4.124402](https://doi.org/10.1103/PhysRevMaterials.4.124402)

I. INTRODUCTION

Potassium titanyl phosphate (KTiOPO_4 , KTP) is a ferroelectric, nonlinear crystal which is commonly applied in optical devices, e.g., for second harmonic generation in solid state lasers. The application in this field is enabled both by a high threshold against optical damage [1,2] and a high optical nonlinearity, mainly caused by distorted TiO_6 octahedra [3] and $\text{K}_{8,9}$ groups [4].

The quality of KTP crystals is impaired by the phenomenon of gray tracking, i.e., photochromic damage [5]. Macroscopically, several mechanisms, like electric fields [1], high intensity laser light [6,7], or exposure to hydrogen at high temperatures [8], are known to lead to their formation. Microscopically, the reduction of Ti atoms near special defects is proposed to cause or at least to facilitate their formation [9]. This hypothesis is supported by the detection of Ti^{3+} centers within KTP crystals using electron paramagnetic resonance (EPR) spectroscopy [1,9,10].

The KTP unit cell contains 64 atoms that are arranged in an orthorhombic crystal lattice; see Fig. 1. These atoms can be reduced to a system of two nonequivalent KTiOPO_4 macromolecules which are related via the symmetry operations of the $Pna2_1$ space group. Therefore, two nonequivalent Ti, P, and K sites as well as ten nonequivalent O sites can be found within the crystal. In addition, the O atoms can be further divided into two groups due to their coordination. The atoms denoted here with O(1)–O(8) are bonded to one Ti and one P atom, and the atoms O(9) and O(10) are bonded to two Ti atoms [2,11–13]. For the notation of the atoms see [13]. As a result, many intrinsic defect configurations become possible.

Setzler *et al.* [10] identified four different Ti^{3+} centers in KTP crystals. Two of these are exclusively found in hydrothermally grown crystals and the other two in crystals grown using a flux method [10]. While the former are caused by a trapped proton (i.e. an OH^- group), the latter are caused by either an oxygen vacancy located between two Ti atoms or by a self-trapped electron. Only the center caused by an oxygen vacancy is stable at room temperatures.

The present study aims to model the paramagnetic defect geometries, which lead both to the formation of Ti^{3+} centers and to the experimentally observed hyperfine splittings. The *ab initio* approach allows one to study selectively the impact of isolated point defects so that a better understanding of the microscopic processes within the crystal can be achieved. By including trapped protons and electrons as well as magnetic signatures, this study complements previous calculations on the energetics of point defects [8,14], while providing a direct comparison with existing experimental data [10].

II. METHODOLOGY

The results discussed in this paper are based on density-functional theory (DFT) as implemented in the open source program QUANTUM ESPRESSO [15,16] (QE). In order to model the electron-ion interactions, norm-conserving pseudopotentials that treat the Ti $3d^3 4s^1$, P $3s^2 3p^3$, K $4s^1$, and O $2s^2 2p^4$ states as valence states are used. The electron exchange and correlation (XC) is described within the generalized gradient approximation (GGA) using the PBEsol functional [17]. For a better description of the strongly localized defect states of the Ti $3d$ shell, the Hubbard correction [18] is applied. The value for the energy correction is calculated using a self-consistent calculation [18] and amounts to 5.1 eV. The wave functions are expanded in plane waves up to an energy cutoff of 100 Ry. The calculations are performed within the 64 atom KTP

^{*}adrianab@mail.upb.de

unit cell using periodic boundary conditions. The small band dispersion allows for restricting the Brillouin zone sampling to the Baldereschi point [19]. In order to model isolated defects in an otherwise perfect crystal, the atomic positions are relaxed while the lattice constants are kept at fixed values of 12.859, 6.432, and 10.599 Å during all the simulations. These values are taken from a previous study [14] and differ only by 0.4% from the experimental data [2]. For all defect structures, including charged defect states, the atomic positions have been relaxed until residual forces and fluctuations in total energy are below 10^{-4} Ry/bohr and 10^{-8} Ry, respectively.

The hyperfine (hf) splittings, i.e., the interaction of the magnetic moments of the electrons with those of the nuclei, are calculated using the QE-GIPAW code [15,16]: Besides dipolar terms responsible for anisotropic contributions, the relativistic hyperfine tensor consists of the isotropic Fermi contact term which requires the magnetization density $m(\vec{r})$ within a sphere of the Thomas radius $r_T = \frac{Ze^2}{mc^2}$ (about ten times the nuclear radius) around the nuclei [20]. Here, Z is the atomic number, e the elementary charge, m the free electron mass, and c the speed of light. Notably the relativistic formulas are consistent with scalar-relativistic wave functions. Within a pseudopotential approach a reconstruction of the all-electron wave functions from the pseudo wave functions is required, but easily realized via the projector augmented wave (PAW) approach [21].

III. HYPERFINE STRUCTURE

Since only $S = \frac{1}{2}$ EPR signals were measured, defects with an odd number of electrons are required to identify defect structures that are compatible with experimental EPR and electron nuclear double resonance (ENDOR) data [10]. As shown in Ref. [14], K vacancies are only energetically stable in a negative charge state, which corresponds to an even number of electrons. For this reason they will not be discussed in this work, although KTP can show a high concentration of K vacancies [11].

Following the results by Setzler *et al.* in Ref. [10], the influence of trapped protons (i.e., OH^- groups), self-trapped electrons as well as oxygen vacancies are investigated (also see Fig. 1). The Ti^{3+} caused by either oxygen vacancies or self-trapped electrons were only found within KTP crystals grown using a flux method. They were denoted with A_{flx} and I_{flx} , respectively. Those centers which are found near a trapped proton are only present in hydrothermally grown KTP and denoted with I_{hyd} and II_{hyd} . Apart from the A_{flx} center that is stable at room temperatures, all the defect signatures vanish at temperatures between 140 and 200 K.

All these defects behave as electron donors that transfer charge to the atoms surrounding the defect. We quantify these charges using a Löwdin analysis [23]. In each cell that contains one of the defects, which reflect the experimental EPR data [10], one designated Ti atom is found to accumulate a fraction between 0.14 and 0.15 of the freed electron within the $3d$ orbital.¹ Thus, this atom can be identified with one of

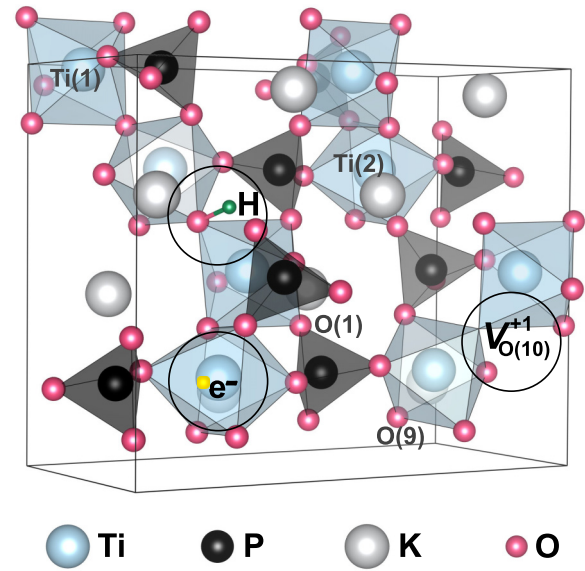


FIG. 1. Schematic illustration [22] of exemplary point defects (i.e., a self-trapped electron, a trapped proton, and the O vacancy $V_{\text{O}(10)}^{+1}$) within the KTP unit cell.

the experimentally detected Ti^{3+} centers. We will first discuss the influence of O vacancies and self-trapped electrons and finally the effects of trapped protons.

A. O vacancies

O vacancies can release up to two electrons [14], but only the charge state +1 provides an unpaired electron giving rise to EPR signals. The behavior of the vacancies at the sites O(1)–O(8) differs from that of the vacancies at the sites O(9) and O(10) due to their coordination. The vacancies belonging to the former class show qualitatively the same behavior so that their discussion is limited to one exemplary vacancy (i.e., $V_{\text{O}(1)}^{+1}$). The vacancies $V_{\text{O}(9)}^{+1}$ and $V_{\text{O}(10)}^{+1}$ are different and will be discussed individually.

After the removal of a Ti–P coordinated O atom, a P dangling bond arises and accumulates most of the released charge [14]. This process has two consequences: First, the defect is characterized by a strong structural relaxation within the +2 and in particular the neutral charge state [14]. Second, the related P atom (with the strongly localized half-filled dangling bond) gives rise to very large hyperfine splittings above 1400 MHz for the vacancy $V_{\text{O}(1)}^{+1}$. Because there is no experimental hint to such high values, these vacancies cannot be related to the experimental EPR spectra. This confirms the observation by Setzler *et al.* [10] who proposed the center A_{flx} to be caused by an O vacancy between two Ti atoms.

The vacancies $V_{\text{O}(9)}^{+1}$ and $V_{\text{O}(10)}^{+1}$ reflect this situation. Providing almost the same total energy, neither configuration

investigate, if the acquired charge leads to the reduction of the Ti atom, we perform a Löwdin analysis [23] for bulk Ti_3O_5 known to host both Ti^{3+} and Ti^{4+} ions [26]. The charge difference between the two ions amounts to $0.18e$, which is of the same order of magnitude as the Ti reduction caused by the defects discussed in this work.

¹The charge of transition metals in compounds is not significantly altered by changes in the formal oxidation state [24,25]. In order to

TABLE I. *Ab initio* calculated and experimental [10] principal values of the hyperfine tensors of the Ti^{3+} centers caused by positively charged oxygen vacancies. The position of the P atoms can be seen in Fig. 2. Note that the vacancies $V_{\text{O}(9)}^{+1}$ and $V_{\text{O}(10)}^{+1}$ lead respectively to the reduction of a Ti(1) and a Ti(2). The former is surrounded by three nonequivalent P atoms, the latter by four, resulting in a respective number of ^{31}P nuclei with a relevant hf splitting.

Nucleus		Expt. [10] A_{flx} Prin. val. (MHz)	Theory	
			$V_{\text{O}(9)}^{+1}$ Prin. val. (MHz)	$V_{\text{O}(10)}^{+1}$ Prin. val. (MHz)
$^{31}\text{P}(1)$	A ₁	16.58	33.73	21.71
	A ₂	16.75	31.50	20.94
	A ₃	23.36	39.64	26.22
$^{31}\text{P}(2)$	A ₁	14.28	1.90	11.73
	A ₂	14.68	1.19	10.95
	A ₃	21.37	3.79	16.84
$^{31}\text{P}(3)$	A ₁	3.74	0.98	2.79
	A ₂	4.24	1.28	1.73
	A ₃	7.23	1.96	4.79
$^{31}\text{P}(4)$	A ₁	0.84		1.76
	A ₂	1.40		0.34
	A ₃	3.94		3.47

leads to the formation of dangling bonds. The released charge is mainly stabilized by the Ti atoms near the vacancy. Unfortunately, the Ti related hyperfine splittings have not been resolved experimentally and thus will not be discussed in the following. The principal values of the hyperfine tensors of the surrounding ^{31}P nuclei are shown in Table I. The comparison with experimentally resolved data shows that the vacancy $V_{\text{O}(10)}^{+1}$ leads to the best agreement by far. Also the experimental suggestion [10] of the position of the Ti^{3+} center at the lattice site Ti(2) is fulfilled by this vacancy exclusively. Comparing the magnetization densities $m(\vec{r}) = n^\uparrow(\vec{r}) - n^\downarrow(\vec{r})$ as a measure for the unpaired electron (see Fig. 2), it becomes clear that the vacancy $V_{\text{O}(10)}^{+1}$ leads to the polarization of two Ti atoms, while in the presence of the vacancy $V_{\text{O}(9)}^{+1}$ only the central Ti^{3+} atom is strongly polarized.

B. Self-trapped electrons

The center I_{flx} was proposed by Setzler *et al.* [10] to be caused by a self-trapped electron at the site Ti(1). In order to differentiate between the two Ti sites, we localize the electron at both sites and relax the atomic positions afterwards.

At first view, the magnetization densities of both models look very similar: It is clearly visible that the trapped electron leads to the polarization of the stabilizing Ti atom; see Fig. 3. However, if the electron is trapped by the atom at the lattice site Ti(1), a second Ti atom is polarized too. This atom is connected to the first by a mutual O(9). In addition, the Ti(1) trapped electron is surrounded by only three nonequivalent P atoms instead of four in the case of Ti(2), resulting in a respective number of ^{31}P related hyperfine splittings; see Table II. Based on the number of experimentally resolved ^{31}P nuclei,

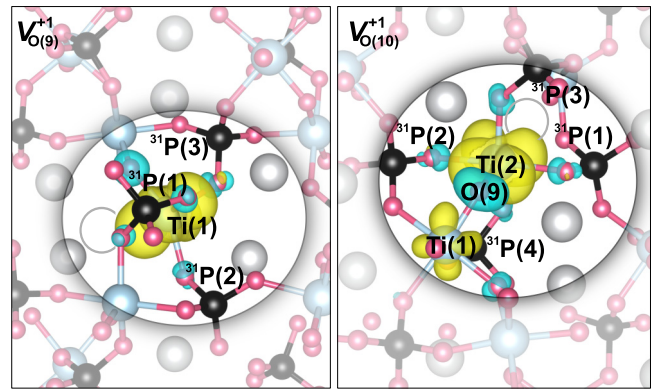


FIG. 2. Magnetization density of the positively charged O vacancies $V_{\text{O}(9)}^{+1}$ (left-hand side) and $V_{\text{O}(10)}^{+1}$ (right-hand side). The position of the vacancy within the cell is shown schematically by the light gray ring. The yellow isosurfaces indicate areas where the majority spin dominates, while the cyan isosurfaces show those areas dominated by the minority spin. The Ti^{3+} caused by the latter can be attributed to the center A_{flx} [10] (also see Table I).

we attribute the EPR-active I_{flx} center to a trapped electron at the Ti(1) site.

C. Trapped protons

The centers I_{hyd} and II_{hyd} arise in hydrothermally grown KTP exclusively and are proposed to be caused by trapped protons [10]. In order to find proper defect models, we aimed not only to reproduce the experimental hyperfine tensors, but also to determine the position of the Ti^{3+} center within the cell. Since the principal values of the hyperfine tensors are very sensitive to the position of the H atom, we could easily distinguish the atomic geometries.

The models that reflect the experiment best are (i) a trapped proton combined with the nearest O vacancy $V_{\text{O}(4)}^0$ for the center I_{hyd} and (ii) a single trapped proton for the center II_{hyd} . The former will be denoted with $\text{H}_i^{\text{O}(4)}$, the latter with H_i . In both cases, the H atom is bound to a Ti-Ti coordinated O atom at

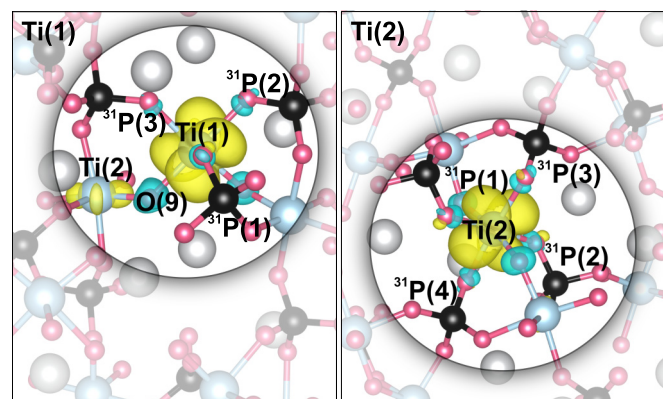


FIG. 3. Magnetization density as a direct measure of the trapped electron at the site Ti(1) (left-hand side) and Ti(2) (right-hand side). The Ti^{3+} caused by the former can be attributed to the center I_{flx} [10] (also see Table II).

TABLE II. *Ab initio* calculated and experimental [10] principal values of the hyperfine tensors of the Ti^{3+} centers caused by self-trapped electrons with three [Ti(1)] and four [Ti(2)] relevant ^{31}P nuclei. The positions of the P atoms can be seen in Fig. 3.

Nucleus		Expt. [10]		Theory	
		I_{fix} Prin. val. (MHz)		Ti(1) Prin. val. (MHz)	Ti(2) Prin. val. (MHz)
$^{31}\text{P}(1)$	A ₁	22.12		20.65	24.22
	A ₂	22.24		19.34	22.97
	A ₃	29.15		27.66	30.29
$^{31}\text{P}(2)$	A ₁	16.61		19.10	21.81
	A ₂	16.74		18.65	20.57
	A ₃	23.45		24.07	29.10
$^{31}\text{P}(3)$	A ₁	5.29		2.87	5.66
	A ₂	6.49		2.05	3.94
	A ₃	10.04		5.32	7.54
$^{31}\text{P}(4)$	A ₁				5.18
	A ₂				3.80
	A ₃				7.50

the site O(9). The length of each O-H bond amounts to 0.99 Å, which is in good agreement with the value of 0.98 Å derived by Setzler *et al.* [10] as the average bond length between the H atom and the nearest Ti-Ti coordinated O atom in the vicinity of the center I_{hyd} .

The calculated hyperfine splittings of the H atom are strongly underestimated for all investigated H including models (see Table III). A possible explanation for the deviation could either be a bias during the experiment or a XC functional induced wrong localization of the unpaired electron within the OH group.

On the other hand, the hyperfine splitting of the ^{31}P nuclei (see Table III) are in quite good agreement with the

TABLE III. *Ab initio* calculated and experimental [10] principal values of the hyperfine tensors of the Ti^{3+} centers caused by trapped protons. The positions of the P atoms are also indicated in Figs. 4 and 5.

Nucleus		Expt. [10]		Theory	
		I_{hyd} Prin. val. (MHz)	$\text{H}_i^{\text{O}(4)}$ Prin. val. (MHz)	I_{hyd} Prin. val. (MHz)	H_i Prin. val. (MHz)
^1H	A ₁	13.87	3.02	9.76	3.57
	A ₂	14.09	0.78	10.71	1.29
	A ₃	26.37	17.44	22.61	17.53
$^{31}\text{P}(1)$	A ₁	22.84	20.84	22.15	20.14
	A ₂	22.94	20.13	22.32	19.11
	A ₃	29.54	30.32	28.38	28.54
$^{31}\text{P}(2)$	A ₁	17.01	19.15	16.36	13.79
	A ₂	17.22	18.41	16.53	12.76
	A ₃	23.05	24.79	23.54	18.72
$^{31}\text{P}(3)$	A ₁	6.89	6.15		0.02
	A ₂	8.10	8.82		0.59
	A ₃	12.03	3.34		1.81

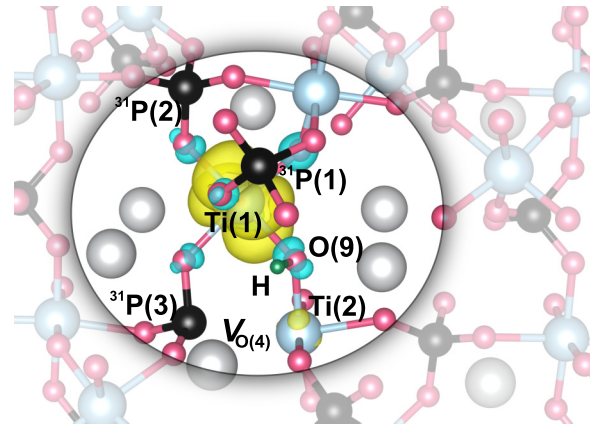


FIG. 4. Magnetization density of the defect complex $\text{H}_i^{\text{O}(4)}$. The defect model can be attributed to the Ti^{3+} center I_{hyd} [10] (also see Table III).

experiment, except for the additional nucleus $^{31}\text{P}(3)$ within the cell containing the single trapped proton H_i . However, given the large anisotropy of the hyperfine tensor, the corresponding hyperfine satellites are less intense and could not be resolved experimentally.

$\text{H}_i^{\text{O}(4)}$ leads to the reduction of the atom at the lattice site Ti(1), as concluded from the experiment. In addition, the defect complex leads to the polarization of two Ti atoms; see Fig. 4. A similar effect has been already mentioned during the discussion of the O vacancies and the self-trapped electrons.

In Ref. [10], the I_{hyd} center has been tentatively attributed to the lattice site Ti(2). Based on our calculated hyperfine splittings for H-related centers, however, this assignment has to be refined: The best agreement with the experimental values is found for the H_i model. Here, as shown in Fig. 5, the magnetization density is located at the reduced Ti(1) atom exclusively contrasting the previous experimental suggestion.

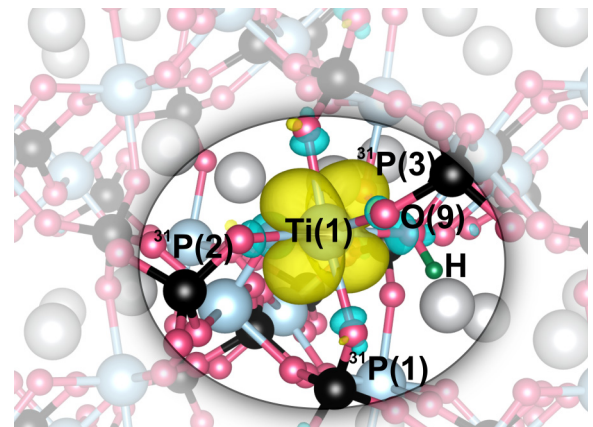


FIG. 5. Magnetization density of the single trapped proton H_i . The defect model can be attributed to the Ti^{3+} center I_{hyd} [10] (also see Table III).

TABLE IV. Separation of the highest defect levels ΔE from the conduction band (PBEsol + U) in comparison to the experimental excitation energy for gray track formation.

	Ti(1)	$V_{O(10)}^{+1}$	$H_i^{O(4)}$	H_i	Expt.
ΔE (eV)	1.28	1.94	1.65	1.63	2.33

IV. POSSIBLE ROLE IN GRAY TRACK FORMATION

KTP crystals are usually characterized by a high transparency in the range between 450 and 3500 nm; see e.g., Ref. [2]. After the formation of gray tracks, the absorption of KTP crystals increases. All simulated defect models provide unpaired electrons and lead to the formation of occupied defect levels within the band gap. The separations ΔE of the highest occupied level from the bottom of the conduction band (PBEsol + U) are compiled in Table IV. A possible explanation for the increased absorption is given by optical excitation of these defect states.

It has been shown that the formation of gray tracks during 1064 nm second harmonic generation (SHG) is related to the intensity of the 532 nm (2.33 eV) radiation [27]. The experimental excitation energy of 2.33 eV is larger than the largest ΔE value calculated here. This may be related to the underestimation of the DFT band gap [28,29] as well as to the fact that the excitation does not necessarily occur to the bottom of the conduction band. Hybrid functionals (HSE [30]) have been tested, but do not alter the excitation energies significantly. Independently of the XC functional, best agreement with experimental data is achieved for the O vacancy $V_{O(10)}^{+1}$.

For this reason and because they lead to the formation of the only thermally stable Ti^{3+} center, we propose that vacancies $V_{O(10)}^{+1}$ provide the best candidate to explain the increase of the absorption of KTP during SHG. Therefore they seem to be directly connected with the phenomenon of gray tracking.

O vacancies easily form in KTP to charge compensate K^+ vacancies [11]. As a matter of fact, crystals with lower K

vacancy concentration are less affected by gray tracking [11] and the transmission of KTP can be increased by annealing the crystal in wet oxygen [31]. Our results are also consistent with the fact that the resistance of a KTP crystal against gray tracking was found to decrease with higher O vacancy concentrations [32,33]. In addition, it has been shown that there is no correlation between the gray tracking susceptibility of a crystal and the concentration of hydroxyl groups [31].

However, if O vacancies are naturally present in KTP, what is the reason why KTP crystals are not always affected by gray tracking?

This question may be answered by analyzing the formation energy of the defect. At the GGA-level of theory [14], it has been shown that O vacancies are energetically stable in the 2+ charge state predominantly. Charge transitions are predicted only close to the conduction bands. We recalculate the formation energy of the vacancy $V_{O(10)}$ using PBEsol + U functionals and the Slater-Janak transition state approach [34]. Thanks to this method, the calculation of the charge transition energies does not require a total-energy comparison of the system with different numbers of electrons. Thus, there is no need for any charge correction schemes.

The application of the Hubbard-correction increases the electron localization and lowers the position of the highest occupied defect level. As a consequence, as shown in Fig. 6, the neutral charge state becomes stable in the upper half of the band gap; the 2+ charge state remains the stable one only for Fermi levels below midgap. The 1+ charge state (which gives rise to EPR signals) becomes also stable, but only for a narrow range of intermediate Fermi level positions.

In KTP crystals Fermi level lowering p -type doping can be achieved by substituting K^+ vacancies with, e.g., Pb^{2+} cations promoting the 2+ charge state. In this charge state, no defect level within the band gap can be found which means that the vacancies $V_{O(10)}^{+2}$ do not influence the absorption properties of KTP. This observation is in agreement with the results by Stevens *et al.* [35], who did not resolve the presence of O-vacancy-related Ti^{3+} centers in Pb-containing KTP crystals and noted an increased transparency, proposing that the gray tracking resistance can be improved by introducing these atoms in the crystal lattice. However, if K^+ vacancies (present in different concentrations in all KTP crystals [11]) are not compensated, they will show a comparable effect as an n -type doping, shifting the Fermi-energy towards the conduction band. Thus, the +1 and the neutral charge state becomes possible.

Setzler *et al.* [10] noticed that the formation of the center A_{flx} corresponds to the decay of the center I_{flx} at a temperature near 140 K. Since a self-trapped electron is quite unstable, the increasing thermal energy can lead to the detachment of the electron. The released electron is then stabilized by a Ti

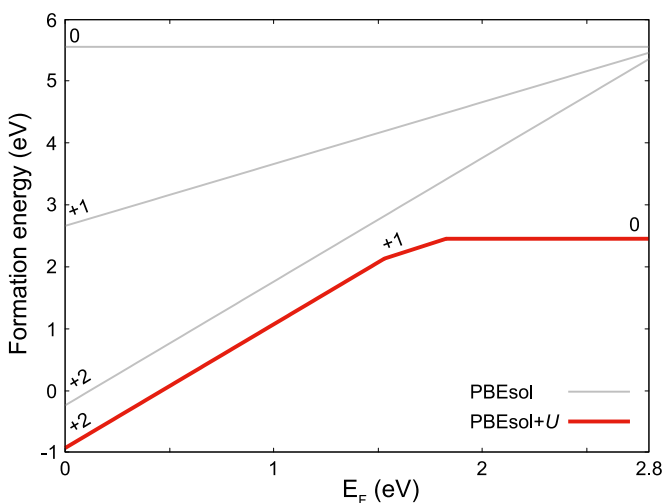


FIG. 6. Calculated $V_{O(10)}$ formation energy in dependence on the Fermi level position using PBEsol [14] and PBEsol + U functionals.

TABLE V. Binding energy of a self-trapped electron and the vacancy $V_{O(10)}$ in the charge state +2 and +1.

	$\Delta E_{\text{bind.}}$ (eV)
$V_{O(10)}^{+2}$ + self-trapped e^-	-0.75
$V_{O(10)}^{+1}$ + self-trapped e^-	-1.02

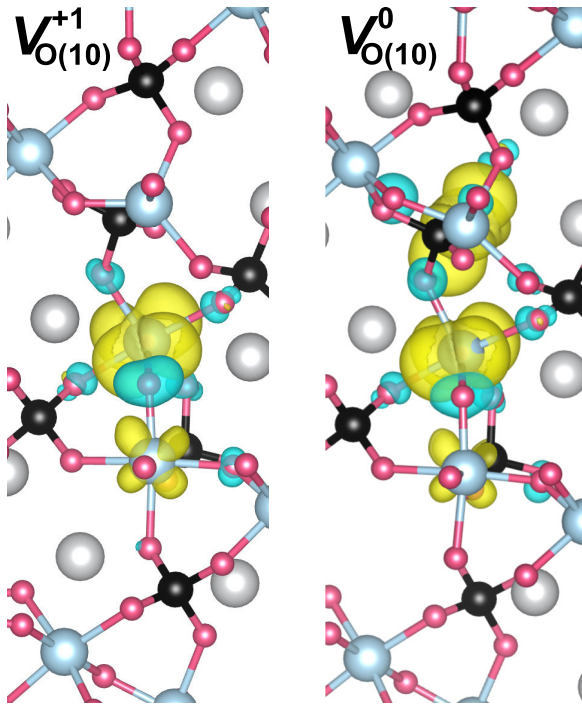


FIG. 7. Comparison between the magnetization densities of the O vacancies $V_{O(10)}^{+1}$ and $V_{O(10)}^0$. The additional electron leads to the formation of a chain of polarized Ti atoms. The binding energy of the second extra electron is larger than the first; see Table V.

atom near an O vacancy $V_{O(10)}^{+2}$ leading to the single positively charged vacancy $V_{O(10)}^{+1}$. In fact, we found that the system is more stable if the extra electron is trapped by a Ti atom nearby an O vacancy, since its binding energy ΔE_{bind} is negative; see Table V. As a consequence, these defects spontaneously form within KTP crystals, giving rise to the midgap defect level. If the concentration of O vacancies is high enough, this level broadens and the formation of gray tracks may be facilitated.

We briefly note that the defect may also trap two electrons. Interestingly, the binding energy of the second electron is 0.27 eV larger than the value of the first; see also Table V. As illustrated in Fig. 7, the stabilization of two electrons leads to the formation of chains of polarized Ti atoms within the crystal and so to a further increase of the anisotropy compared to the charge state +1. If the concentration of vacancies $V_{O(10)}^0$ is high enough, these chains may connect and extend through the entire crystal. We speculate that these macroscopic chains of polarized Ti atoms may interfere with the irradiating light. Regarding the hyperfine splittings of the P atoms, we found that the values of the $S = 1$ spin triplet are similar to the values of the vacancy $V_{O(10)}^{+1}$. The overall EPR fingerprint should be

clearly distinct from the experimental observed $S = \frac{1}{2}$ spectra, but will require optical excitation at least in standard, moderately doped KTP samples.

V. CONCLUSION

In this work different paramagnetic point defects in KTP (i.e., self-trapped electrons, positively charged O vacancies, and trapped protons) were studied within density-functional theory (DFT) with respect to their magnetic and electronic properties. The simulated defects behave as electron donors and induce polarons in the KTP lattice. Thereby, the released electron is mainly stabilized by one Ti atom in the vicinity of the defect. As a consequence, this atom changes its formal oxidation state from 4+ to 3+.

Defect induced Ti^{3+} centers in KTP are commonly related to the phenomenon of gray tracking, which impairs the properties of the crystal. Within these *ab initio* calculations the microscopic effects of every simulated defect could be analyzed. It is found that only four models can explain the results of a previous EPR and ENDOR study by Setzler *et al.* [10]. A positively charged O vacancy at the lattice site $\text{O}(10)$ $V_{O(10)}^{+1}$ can be attributed to the only thermally stable Ti^{3+} center. Comparing the position of the highest occupied defect level of each defect model with the experimental excitation energy, it is also found that the vacancy $V_{O(10)}^{+1}$ explains best the increase of the absorption of KTP during 1064 nm SHG.

By analyzing the formation energy of the charged vacancy $V_{O(10)}$, it is found that the role of K^+ vacancies (or rather their compensation with a *p*-type dopant) is crucial for the EPR active +1 charge state. In fact, for low K^+ vacancy concentrations the vacancy $V_{O(10)}^{+2}$ is more likely to form. In this charge state, the vacancy does not feature a midgap defect level so it does not influence the absorption properties of KTP.

In addition, O vacancies may also stabilize a second electron leading to the formation of polarized Ti atoms connected into chains, which may interfere with the irradiating light field, further facilitating the observed damage.

A thorough understanding of the Ti^{3+} centers should be beneficial to circumvent the photochromic damage. However, further investigations both theoretical and experimental are required to confirm the developed scenario of gray tracking.

ACKNOWLEDGMENTS

The authors gratefully acknowledge financial support from the Deutsche Forschungsgemeinschaft (DFG) via Sonderforschungsbereich TRR 142, Project No. 231447078, and computational resources provided by the Paderborn Center for Parallel Computing (PC²) and the High Performance Computing Center Stuttgart (HLRS).

- [1] M. G. Roelofs, *J. Appl. Phys.* **65**, 4976 (1989).
- [2] J. D. Bierlein and H. Vanherzeele, *J. Opt. Soc. Am. B* **6**, 622 (1989).
- [3] F. C. Zumsteg, J. D. Bierlein, and T. E. Gier, *J. Appl. Phys.* **47**, 4980 (1976).

- [4] D. Xue and S. Zhang, *Appl. Phys. Lett.* **70**, 943 (1997).
- [5] Q. Zhang, G. Feng, J. Han, B. Li, Q. Zhu, and X. Xie, *Optik* **122**, 1313 (2011).
- [6] B. Boulanger, I. Rousseau, J. P. Feve, M. Maglione, B. Menaert, and G. Marnier, *IEEE J. Quantum Electron.* **35**, 281 (1999).

- [7] V. A. Maslov, V. A. Mikhailov, O. P. Shaunin, and I. A. Shcherbakov, *Quantum Electron.* **27**, 356 (1997).
- [8] Y. Zhang, Y. Leng, J. Liu, N. Ji, X. Duan, J. Li, X. Zhao, J. Wang, and H. Jiang, *CrystEngComm* **17**, 3793 (2015).
- [9] M. P. Scripsick, G. J. Edwards, L. E. Halliburton, R. F. Belt, and G. M. Loiacono, *J. Appl. Phys.* **76**, 773 (1994).
- [10] S. D. Setzler, K. T. Stevens, N. C. Fernelius, M. P. Scripsick, G. J. Edwards, and L. E. Halliburton, *J. Phys. Condens. Matter* **15**, 3969 (2003).
- [11] M. Roth, in *Springer Handbook of Crystal Growth*, edited by G. Dhanaraj, K. Byrappa, V. Prasad, and M. Dudley (Springer, Berlin, 2010), Chap. 20, pp. 691–723.
- [12] N. I. Sorokina and V. I. Voronkova, *Crystallogr. Rep.* **52**, 80 (2007).
- [13] J. E. Lowther, P. Manyum, and P. Suebka, *Phys. Status Solidi B* **242**, 1392 (2005).
- [14] A. Bocchini, S. Neufeld, U. Gerstmann, and W. G. Schmidt, *J. Phys. Condens. Matter* **31**, 385401 (2019).
- [15] P. Giannozzi, S. Baroni, N. Bonini, M. Calandra, R. Car, C. Cavazzoni, D. Ceresoli, G. L. Chiarotti, M. Cococcioni, I. Dabo, A. D. Corso, S. de Gironcoli, S. Fabris, G. Fratesi, R. Gebauer, U. Gerstmann, C. Gougoussis, A. Kokalj, M. Lazzeri, L. Martin-Samos *et al.*, *J. Phys. Condens. Matter* **21**, 395502 (2009).
- [16] P. Giannozzi, O. Andreussi, T. Brumme, O. Bunau, M. B. Nardelli, M. Calandra, R. Car, C. Cavazzoni, D. Ceresoli, M. Cococcioni, N. Colonna, I. Carnimeo, A. D. Corso, S. de Gironcoli, P. Delugas, R. A. DiStasio, A. Ferretti, A. Floris, G. Fratesi, G. Fugallo *et al.*, *J. Phys. Condens. Matter* **29**, 465901 (2017).
- [17] J. P. Perdew, A. Ruzsinszky, G. I. Csonka, O. A. Vydrov, G. E. Scuseria, L. A. Constantin, X. Zhou, and K. Burke, *Phys. Rev. Lett.* **100**, 136406 (2008).
- [18] M. Cococcioni and S. de Gironcoli, *Phys. Rev. B* **71**, 035105 (2005).
- [19] A. Baldereschi, *Phys. Rev. B* **7**, 5212 (1973).
- [20] S. Blügel, H. Akai, R. Zeller, and P. H. Dederichs, *Phys. Rev. B* **35**, 3271 (1987).
- [21] C. G. Van de Walle and P. E. Blöchl, *Phys. Rev. B* **47**, 4244 (1993).
- [22] K. Momma and F. Izumi, *J. Appl. Crystallogr.* **44**, 1272 (2011).
- [23] P.-O. Löwdin, *Phys. Rev.* **97**, 1474 (1955).
- [24] D. Koch and S. Manzhos, *J. Phys. Chem. Lett.* **8**, 1593 (2017).
- [25] D. Koch and S. Manzhos, *J. Phys. Chem. Lett.* **8**, 3945 (2017).
- [26] C. Schlenker, R. Buder, M. Schlenker, J. F. Houlihan, and L. N. Mulay, *Phys. Status Solidi B* **54**, 247 (1972).
- [27] B. Boulanger, M. M. Fejer, R. Blachman, and P. F. Bordui, *Appl. Phys. Lett.* **65**, 2401 (1994).
- [28] P. J. Hasnip, K. Refson, M. I. J. Probert, J. R. Yates, S. J. Clark, and C. J. Pickard, *Philos. T. R. Soc. A* **372**, 20130270 (2014).
- [29] S. Neufeld, A. Bocchini, U. Gerstmann, A. Schindlmayr, and W. G. Schmidt, *J. Phys. Mater.* **2**, 045003 (2019).
- [30] J. Heyd, G. E. Scuseria, and M. Ernzerhof, *J. Chem. Phys.* **118**, 8207 (2003).
- [31] G. M. Loiacono, D. N. Loiacono, T. McGee, and M. Babb, *J. Appl. Phys.* **72**, 2705 (1992).
- [32] K. Terashima, M. Takena, and M. Kawachi, *Jpn. J. Appl. Phys.* **30**, L497 (1991).
- [33] Y. Zhang, J. Li, X. Cao, J. Yang, J. Wang, and H. Jiang, *AIP Adv.* **4**, 127103 (2014).
- [34] S. Sanna, T. Frauenheim, and U. Gerstmann, *Phys. Rev. B* **78**, 085201 (2008).
- [35] K. T. Stevens, L. E. Halliburton, M. Roth, N. Angert, and M. Tseitlin, *J. Appl. Phys.* **88**, 6239 (2000).